Normalized metal artifact reduction (NMAR) in computed tomography

Esther Meyer[a)]
Institute of Medical Physics, University of Erlangen–Nürnberg, D-91052 Erlangen, Germany and Siemens Healthcare Forchheim, D-91301 Forchheim, Germany

Rainer Raupach
Siemens Healthcare Forchheim, D-91301 Forchheim, Germany

Michael Lell
Institute of Diagnostic Radiology, University of Erlangen–Nürnberg, D-91054 Erlangen, Germany

Bernhard Schmidt
Siemens Healthcare Forchheim, D-91301 Forchheim, Germany

Marc Kachelrieß
Institute of Medical Physics, University of Erlangen–Nürnberg, D-91052 Erlangen, Germany

(Received 19 May 2010; revised 22 July 2010; accepted for publication 10 August 2010; published 28 September 2010)

Purpose: While modern clinical CT scanners under normal circumstances produce high quality images, severe artifacts degrade the image quality and the diagnostic value if metal prostheses or other metal objects are present in the field of measurement. Standard methods for metal artifact reduction (MAR) replace those parts of the projection data that are affected by metal (the so-called metal trace or metal shadow) by interpolation. However, while sinogram interpolation methods efficiently remove metal artifacts, new artifacts are often introduced, as interpolation cannot completely recover the information from the metal trace. The purpose of this work is to introduce a generalized normalization technique for MAR, allowing for efficient reduction of metal artifacts while adding almost no new ones. The method presented is compared to a standard MAR method, as well as MAR using simple length normalization.
Methods: In the first step, metal is segmented in the image domain by thresholding. A 3D forward projection identifies the metal trace in the original projections. Before interpolation, the projections are normalized based on a 3D forward projection of a prior image. This prior image is obtained, for example, by a multithreshold segmentation of the initial image. The original rawdata are divided by the projection data of the prior image and, after interpolation, denormalized again. Simulations and measurements are performed to compare normalized metal artifact reduction (NMAR) to standard MAR with linear interpolation and MAR based on simple length normalization.
Results: Promising results for clinical spiral cone-beam data are presented in this work. Included are patients with hip prostheses, dental fillings, and spine fixation, which were scanned at pitch values ranging from 0.9 to 3.2. Image quality is improved considerably, particularly for metal implants within bone structures or in their proximity. The improvements are evaluated by comparing profiles through images and sinograms for the different methods and by inspecting ROIs. NMAR outperforms both other methods in all cases. It reduces metal artifacts to a minimum, even close to metal regions. Even for patients with dental fillings, which cause most severe artifacts, satisfactory results are obtained with NMAR. In contrast to other methods, NMAR prevents the usual blurring of structures close to metal implants if the metal artifacts are moderate.
Conclusions: NMAR clearly outperforms the other methods for both moderate and severe artifacts. The proposed method reliably reduces metal artifacts from simulated as well as from clinical CT data. Computationally efficient and inexpensive compared to iterative methods, NMAR can be used as an additional step in any conventional sinogram inpainting-based MAR method. [DOI: 10.1118/1.3484090]

Key words: metal artifact reduction, metal artifact correction, metal artifacts, image quality, sinogram inpainting

I. INTRODUCTION

I.A. Overview

Modern CT scanners are able to produce high quality images, and under ideal circumstances (a water cylinder in a well-calibrated scanner), CT values can reach an accuracy of 1 HU.[1] However, if metal objects are present in the field of measurement, severe artifacts with a magnitude of up to several hundred HU degrade the image quality and diagnostic value.

There are various effects that lead to the formation of artifacts in the presence of metal objects. Metals have much higher densities and higher atomic numbers compared to body tissue. Also, metal implants usually have sharply defined boundaries. Because of these reasons, noise, beam hardening artifacts, scatter artifacts, and nonlinear partial volume artifacts are much more severe than in cases without metal. The term *metal artifact* is a generic term for all of these artifacts.

Low-contrast structures may be easily obscured by metal artifacts. Tumors in the tongue, for example, might remain undetected in the presence of dental fillings. Additional scans with higher tube current and higher tube voltage or with a patient position avoiding metal implants in the scan plane might be necessary. Thus, the patient dose is increased.

Various types of metal artifact reduction (MAR) methods have been proposed since the first publications on MAR.[2,3] They can be grouped into sinogram inpainting methods, iterative methods, statistical methods, and filtering methods. To our knowledge, no commercially available CT scanner is currently providing metal artifact reduction software, and therefore, metal implants remain a major source of artifacts in computed tomography.

Sinogram inpainting methods, which are most common MAR methods, use interpolation[3–5] or forward projections[6–8,24] to complete the sinogram, where metal-affected values are treated as missing data. Filtering methods try to make use of all the available information and not to replace parts of projections.[9,10] Iterative methods provide a means of incorporating additional knowledge, as, for example, the physics behind the acquisition process or photon statistics.[11–14] Statistical methods are less sensitive to noise than filtered backprojection. As shown in Ref. 15, a combination of different methods can be advantageous. Another interesting approach that has been pursued is MAR with total variation minimization.[16]

I.B. Sinogram inpainting

Sinogram inpainting methods, which are most widely spread among MAR methods, treat those parts of the projection data that are affected by metal (the so-called metal trace or metal shadow) as missing data. The underlying idea is to consider any sinogram values as completely unreliable if the corresponding rays have intersected metal objects.

These methods make use of interpolation[3–5] or forward projection[6–8] to complete the sinogram by inpainting the surrogate data into the metal trace. The simplest example is linear interpolation in the channel direction, as proposed in Ref. 3. This method is referred to as MAR1 this work. Metal is found by a thresholding operation in the uncorrected image. The metal-only image is subject to a forward projection. Nonzero entries in the obtained metal sinogram define the metal trace, which determines the part of the original rawdata that has to be replaced. After interpolation, the image is reconstructed. A major drawback of pure interpolation methods is the loss of information, especially edge information in the metal trace, which results in blurring of the corresponding edges in the image. Another negative effect is the formation of streak artifacts tangent to metal objects, which are introduced if the transition between original and interpolated projection data is not smooth enough.[17] These effects are most prominent in regions close to metal objects because a greater part of surrogate sinogram values contributes here. The severely reduced image quality close to implants is especially disturbing when the prostheses are related to the reason for scheduling a patient for CT. It is therefore necessary to pay attention to the proximity of metal objects and to avoid the creation of new artifacts there. Besides linear interpolation (MAR1), many different and more complex interpolation schemes have been applied in order to obtain more accurate surrogate data. For example, distance weighted, directional, spline vs. Fourier-based, and smooth interpolation have been investigated in Refs. 4 and 18–21. The problem itself—the loss of information in the metal trace and hence the introduction of new artifacts—remains the same.

In Ref. 17, a length normalization of the sinogram prior to interpolation is used to obtain better contrast between air and objects of water-equivalent material. This method is referred to as MAR2 in this work. However, regions close to bone structures and between bone and metal are still impaired. This work introduces the normalized metal artifact reduction (NMAR) to overcome these drawbacks.[22]

II. METHOD

II.A. Idea

In this work, it is shown how typical drawbacks of pure sinogram interpolation methods are overcome with normalized metal artifact reduction (NMAR). One problem with interpolation in the sinogram is the lack of smoothness of the transition region from original to interpolated data, which causes streak artifacts. Interpolation is less problematic in homogeneous data. The idea of a proper normalization is to transform the sinogram in a way that it becomes comparatively flat. If the interpolation is performed on a nearly flat, normalized sinogram, the transition between original data and interpolated values is very smooth.

One way to transform a sinogram into a more homogeneous form is described in Ref. 17. This method is referred to as MAR2 in this work. In the first step, an uncorrected image is reconstructed. The metal trace is determined exactly as for MAR1 (thresholding and forward projection of metal). The uncorrected sinogram is then normalized by dividing each entry by the intersection length of its corresponding ray and the scanned object. The metal projections determine where data in the normalized sinogram are replaced by interpolation (for example linear interpolation). Subsequently, the corrected sinogram is obtained by denormalization. This is done by multiplying the interpolated and normalized sinogram with the intersection lengths again. Reconstruction of this corrected sinogram yields the corrected image.

In contrast to MAR1, MAR2 leads to exact results for the simple case of objects that only consist of one material plus air and metal: Projection values $p=\mathsf{R}f$ (with $\mathsf{R}f$ being the Radon transform or x-ray transform of the scanned object f)

depend not only on the attenuation coefficients of the materials that f consists of but also on the intersection length of the rays with the material. The sinogram of an object consisting only of metal, one material other than metal and air, would attain an average attenuation value everywhere outside the metal trace if each projection value was divided by the corresponding intersection length. These lengths can be computed by the forward projection of a binarized version of the considered object, which can be found by thresholding. After the division, interpolation of the metal trace is carried out. The whole sinogram now attains an average attenuation value everywhere. The sinogram is multiplied with the intersection lengths afterward.

MAR2 leads to excellent results for cases without high contrast. However, in the presence of bones, the normalization with intersection lengths does not lead to a very flat sinogram and new artifacts cannot be avoided. To generalize this idea to more materials, NMAR uses a prior image f^{prior}, which takes bone and potentially other high-contrast structures into account, too.

Another drawback of pure interpolation methods, as mentioned in the previous section, is the loss of edge information in the metal trace, especially for high-contrast structures. With denormalization, as described later in this section, NMAR restores traces of high-contrast objects in the metal shadow. The information of the shape of these traces is contained in the sinogram of the prior image. In contrast to just replacing sinogram values by sinogram values of the prior image, NMAR ensures a seamless fit of the surrogate data and a recovery of traces of objects that are contained in the prior image. At the same time, the interpolation at least approximately connects the traces that are not included in the sinogram of the prior image and which therefore were not completely flattened in the normalized sinogram.

II.B. Algorithm

Figure 1 provides a diagram of the different steps of NMAR. From the original rawdata, an uncorrected image is reconstructed. By thresholding, the metal image is obtained. The prior image is computed by segmentation of soft tissue and bone. Forward projection yields the corresponding sinograms. The original sinogram is then normalized by dividing it by the forward projected prior image. The division is carried out pixelwise. A small positive value t_{eps} has to be chosen as threshold for performing the division in order to not divide by zero. Strictly speaking, only the values close to the metal trace need to be normalized and denormalized because only those contribute to the interpolation. The normalized projections p^{norm} are subject to an interpolation-based MAR operation M (MAR1 in this work). Subsequently, the corrected sinogram p^{corr} is obtained by denormalization of the interpolated, normalized sinogram. This is done by multiplying it with the projection values p^{prior},

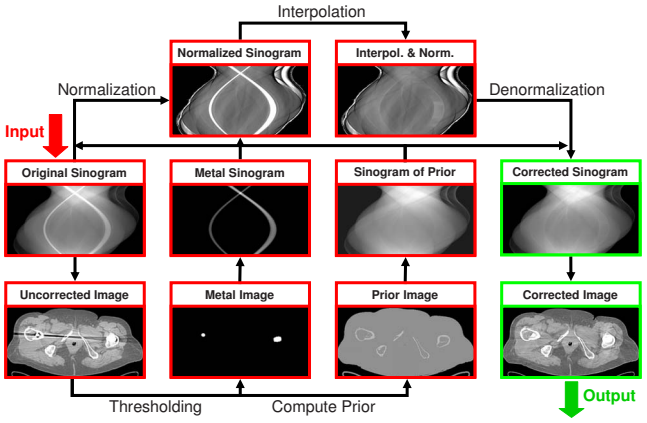

FIG. 1. Scheme of NMAR—From the original rawdata, an uncorrected image is reconstructed. By thresholding, the metal image and the prior image are obtained. Forward projection yields the corresponding sinograms. The original sinogram is then normalized by dividing it by the sinogram of the prior. The metal projections determine where data in the normalized sinogram are replaced by interpolation. The interpolated and normalized sinogram is denormalized by multiplying it with the sinogram of the prior image again. Reconstruction yields the corrected image.

$$p^{\text{corr}} = p^{\text{prior}}\mathsf{M}p^{\text{norm}} = p^{\text{prior}}\mathsf{M}\frac{p}{p^{\text{prior}}} = \mathsf{R}f^{\text{prior}}\mathsf{M}\frac{p}{\mathsf{R}f^{\text{prior}}}.$$

In this step, the structure information from the prior image is brought back to the metal trace. Traces of high-contrast objects are contained in the sinogram of the prior image. The normalization and multiplication procedure ensures that there is no offset between original and completed data. Traces of low-contrast objects in soft tissue that are not included in the prior image, for example tumors, are still approximately connected by interpolation of the normalized sinogram. After reconstruction, the metal is inserted back into the corrected image. This is done for NMAR, as well as for MAR1 and MAR2.

In order to explain the effect of the different steps of NMAR and their difference from MAR2, Fig. 2 shows a correction with NMAR and MAR2 using the example of the simulated hip phantom. Images and the corresponding sinograms are shown and profiles through the sinograms are compared.

For a reliable replacement of the metal projections, the forward projections need to be performed in 3D, in the exact geometry of the uncorrected projections. A 3D version of the Joseph method is used. The Joseph forward projector is a ray-driven forward projector that applies the trapezoidal rule to approximate line integrals through the volume. The values at the sampling points are determined by linear interpolation between the grid points of the discrete volume.[23] To obtain sufficient accuracy of the forward projection, slices of 1.2 mm thick were reconstructed on 0.6 mm increment for the patients scanned with the Definition Flash scanner (slices of 1 mm thick and 1 mm increment for the patient scanned with the Sensation 16 scanner). To reduce aliasing, an aperture of two is simulated by threefold oversampling in the channel direction, i.e., three rays per detector pixel are averaged.

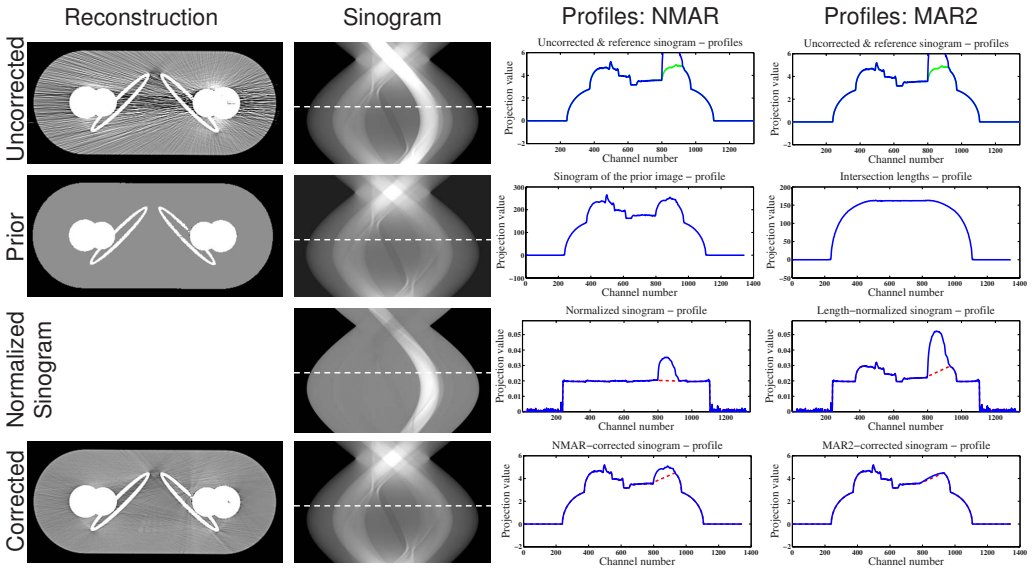

FIG. 2. In order to illustrate the steps of NMAR and their difference from MAR2, images, the corresponding sinograms and profiles through sinograms are shown for the hip phantom. Correction results for MAR1 and MAR2 are found in Fig. 5. The uncorrected data are shown in the top row, the correction results at the bottom row. The column on the right hand side shows profiles of the sinograms of the corresponding steps of MAR2. For NMAR, the normalized sinogram is obtained by dividing the uncorrected sinogram by the sinogram of the prior image (second row). For MAR2, each entry of the uncorrected sinogram is divided by the intersection length (second row) of the corresponding ray and the scanned object. Third row: The dashed lines in the profiles indicate the linearly interpolated values in the metal trace. The MAR2 profile is more homogeneous than the original data, but the bone traces are still visible. The NMAR profile is even more homogeneous than the MAR2 profile. Bottom row: Denormalization of the interpolated profiles yields the corrected data. The solid curves in the graphs are the corrected profiles, while the dashed curves show the MAR1 result for comparison. Both the MAR2 and the NMAR results are smoother than the MAR1 result. The MAR2 result, however, has less accurate values in the bone trace. (C=0 HU/W=1000 HU).

For MAR1, MAR2, and NMAR, a 3D forward projection has to be computed first to identify the metal shadow. Due to the need for projection data of the prior image, NMAR has some additional computational cost compared to pure interpolation methods like MAR1. However, the extra costs are marginal: Merely sinogram values close to and inside the metal trace are needed for normalization and denormalization. Thus, depending on the size of the implants, only very small parts of the prior image have to be forward projected. One additional reconstruction is needed for NMAR if a precorrection with MAR1 is used.

II.C. Prior image

An important step for NMAR is to find a good prior image. It should model the images as close as possible, but contain no artifacts. In order to achieve this, air regions, soft tissue regions, and bone regions have to be identified. In this work, a simple thresholding was applied to segment air, soft tissue, and bone after the image was smoothed with a Gaussian. To reduce the streak artifacts prior to the segmentation, smoothing in the metal trace, as described in Ref. 17, is also beneficial. An automatic procedure to find proper thresholds is described in Ref. 7. The air regions are then set to −1000 HU, the soft tissue parts to 0 HU. Bone pixels keep their values, as they vary too much to properly model them with one value. The value that is assigned to metal is arbitrary. It does not affect the normalization and interpolation because only the sinogram parts close to, but not inside, the metal trace contribute. In the corrected image, the original metal values are finally reinserted to visualize the implants.

For smaller metal objects of medium density, segmentation can be performed in the uncorrected image. NMAR has the advantage that correction results are not impaired compared to the uncorrected images for volume slices only displaying minor artifacts with just few and small metal implants. This is often the case with MAR1 and MAR2, where the regions close to metal are blurred. More details are provided in the next section. For high artifact content, more reliable results are obtained by segmenting bones from an image that is precorrected, for example, with MAR1. Patients 2 and 3 were precorrected with MAR1. In this case, an MAR1 corrected image is reconstructed first. In these cases, NMAR comprises three reconstructions instead of two. Other methods for precorrection can be used, of course.

III. SIMULATIONS AND MEASUREMENTS

III.A. Simulations

To evaluate the potential of NMAR, scans of phantoms for two clinical situations where metal artifacts occur are simulated: Hip replacement by titanium prostheses and spinal fusion using pedicle screws. Semianthropomorphic software phantoms from the FORBILD group (http://www.imp.uni-erlangen.de/phantoms/) were simulated using DRASIM (Siemens Healthcare, Forchheim, Germany). The geometry of the phantoms is presented in Fig. 3. Simulations of the phantoms without metal and without noise are displayed in Fig. 3, too, and serve as reference. Noise, beam hardening, and nonlinear partial volume effects are taken into account during simulation. Realistic material composi-

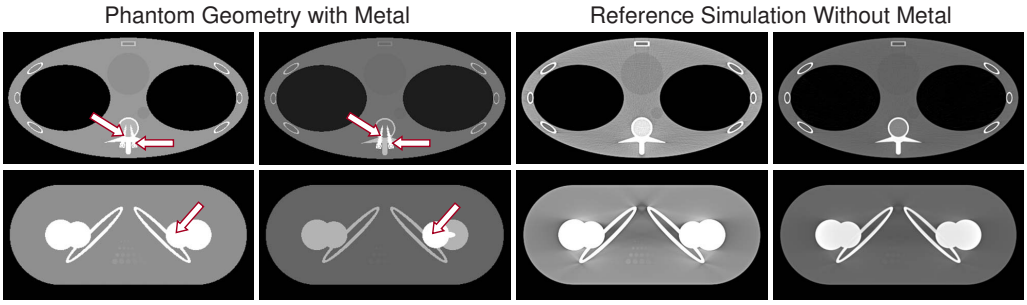

FIG. 3. FORBILD hip phantom and FORBILD thorax phantom. The arrows mark the position of the metal implants. On the left hand side, the geometry of the phantoms is presented. On the right hand side, simulations of the phantoms without metal and without noise are displayed. (C=0 HU/W=1000 HU) and (C=500 HU/W=2500 HU).

tions for soft tissues and bone tissues are simulated. Simulation parameters were 120 kV, 0.6 mm slice width, 672 channels, and 1160 views per rotation. To have a finite beam width, 25 rays per detector element were simulated.

III.B. Measurements

To demonstrate the benefits of NMAR in comparison to MAR1 and MAR2, results for four patients are presented in this work, scanned at pitch values ranging from 0.9 to 3.2. Uncorrected images of each patient are shown in Fig. 4. Patient 1 is a case with bilateral hip endoprostheses. Patient 2 has one hip total endoprosthesis, while patient 3 has metallic dental fillings. The spine of patient 4 is fixed with a Harrington rod. The scan of patient 1 was acquired with a Somatom Sensation 16 (140 kV, 320 mA s, 16×0.75 mm collimation, and 1.0 spiral pitch). Patients 2–4 were acquired with a Somatom Definition Flash scanner. This scanner is a third generation clinical dual source scanner with 64 detector rows per detector, flying focal spot and allows for pitch values up to 3.4.

IV. RESULTS

Results for simulations and clinical data sets, corrected with MAR1, MAR2, and NMAR, are presented in this section. Solid arrows are used to highlight the position of artifacts that are introduced by a correction method. For comparison, outlined arrows mark the same position in an image that does not show an artifact there, and thus imply that the used correction method is superior. The metal artifacts in the uncorrected images, streaks which go through metal, are obvious. Arrows in the uncorrected images mark the position of the metal parts. The results for the patients are presented in two window settings—a narrow window for a better evaluation of streak artifacts and a wider window in order to examine bones and the location and shape of the metal implants.

IV.A. Simulation

Reconstructions of the simulated hip phantom and the simulated thorax phantom, without correction and corrected with MAR1, MAR2, and NMAR are displayed in Fig. 5. The original streak artifacts are removed successfully by each method. However, MAR1 leads to severe new artifacts in both cases: Blurring of the bone near the implant due to loss of edge information and streak artifacts tangent to the former region of the implant. Compared to MAR1, MAR2 visibly enhances image quality for the thorax phantom, but not for the hip phantom. In the thorax phantom, the lungs are filled with air. The binary image, which is used with MAR2 to compute the intersection lengths, contains the information about the shape of the lungs. Therefore, artifacts that are introduced by errors in the traces of the lungs can be avoided. Artifacts close to bones are still present after the correction with MAR2. After correction with NMAR, images exhibit considerably less artifacts for both phantoms. The simulations show that even fine bone structures can be preserved.

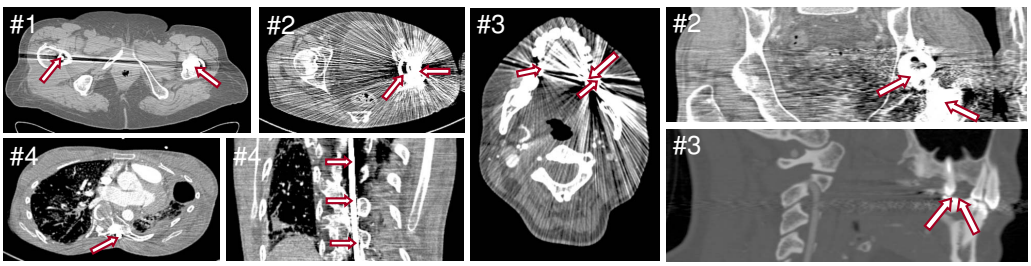

FIG. 4. The four patients considered in this work. Patient 1: Bilateral hip prostheses (C=0 HU/W=500 HU). Patient 2: Unilateral hip prosthesis (C=0 HU/W=500 HU). Patient 3: Dental fillings (C=100 HU/W=750 HU) and (C=300 HU/W=1500 HU). Patient 4: Harrington rod for spine fixation (C=0 HU/W=1000 HU). The arrows mark the locations of the metal implants.

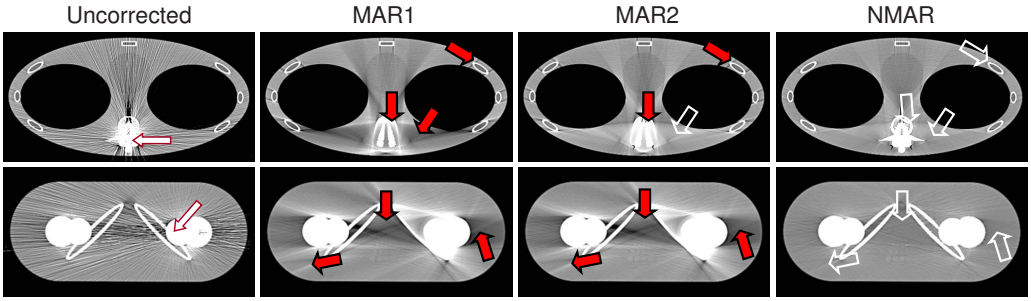

FIG. 5. Comparison for the hip phantom and the thorax phantom. The arrows in the uncorrected images mark the position of the metal implants. In the corrected images, the solid arrows highlight the position of artifacts that are introduced by a correction method. Outlined arrows mark the same position in an image which does not show an artifact there, and thus imply that the used correction method is superior. The original streak artifacts are successfully corrected by each method. However, MAR1 and MAR2 introduce new artifacts. Images exhibit considerably less artifacts after performing NMAR and the simulations show that even fine bone structures can be preserved (C=0 HU/W=500 HU).

IV.B. Measurements

IV.B.1. Patient 1

For patient 1, the patient with two implants, the results are shown in Fig. 6. The uncorrected image suffers from fine streak artifacts and a prominent beam hardening artifact between the two implants. MAR1, MAR2, and NMAR all remove these artifacts. However, MAR1 introduces spurious streaks tangent to the implants. MAR2 introduces them, too, but some are less severe. MAR1 and MAR2 also result in blurring, which is most severe in the upper region of the bone around the prosthesis on the right hand side. Only NMAR results in an image where almost no new streaks are introduced and also does not blur the region close to the implants. The bone surrounding the prostheses is clearly visible after NMAR.

IV.B.2. Patient 2

The images of patient 2, a patient with a hip prosthesis, presented in Figs. 7–9, exhibit much stronger artifacts. All three MAR methods clearly lead to better image quality in the whole volume. Slices in which the metal consists of a single object with a round cross section, as shown in Fig. 7, are the ideal case for interpolation-based MAR. Still, there are improvements of MAR2 and NMAR compared to MAR1. Correction with MAR2 and NMAR leads to a more homogeneous result and less artifacts tangent to the prosthesis. After correction with MAR2, however, some dark artifacts close to the bone structures are visible. They are the consequence of too low sinogram values in the metal trace, as MAR2 does not account for the higher attenuation of the bone tissue. In Fig. 8, the described effects are more pronounced, as the cross section of the metal is greater.

The results for a slice intersecting the very end of the fixation of the prosthesis are shown in Fig. 9. The artifacts in the uncorrected image are very mild. However, if the whole volume is corrected, this slice is corrected as well. The correction results for MAR1 and MAR2 are worse than the uncorrected version; the fine bone structures close to the fixation are blurred. In the NMAR corrected image, blurring and streak artifacts are no longer visible.

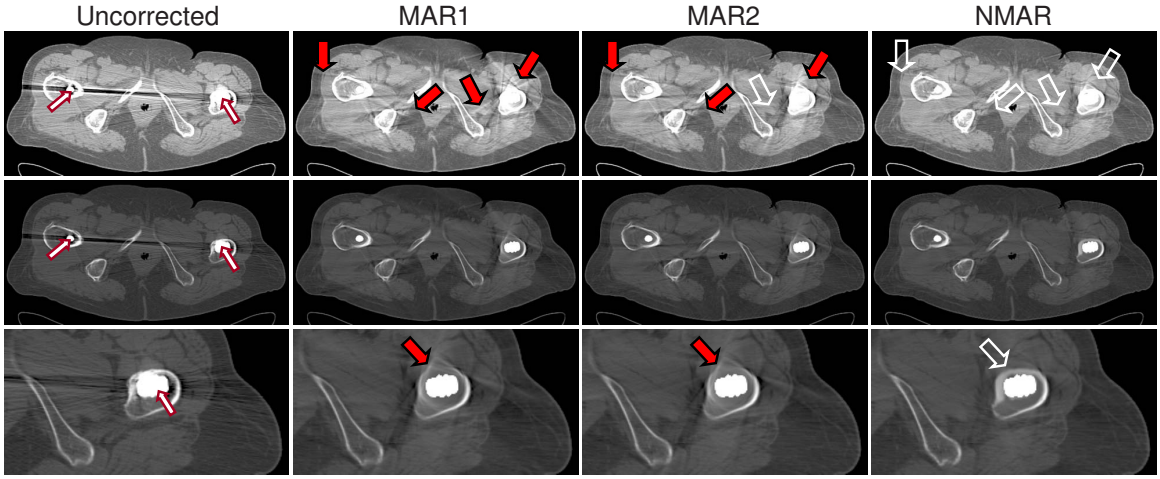

FIG. 6. Patient 1 with bilateral hip endoprostheses. Arrows in analogy to Fig. 5. MAR1 and MAR2 result in blurring of bone and introduce streak artifacts. New streak artifacts are slightly reduced with MAR2 compared to MAR1. NMAR results in an image with almost no new streaks. The magnification at the bottom row shows that the bone surrounding the right hand side of the prosthesis is clearly visible only after NMAR. Top row: (C=0 HU/W=500 HU). Middle and bottom row: (C=500 HU/W=1500 HU).

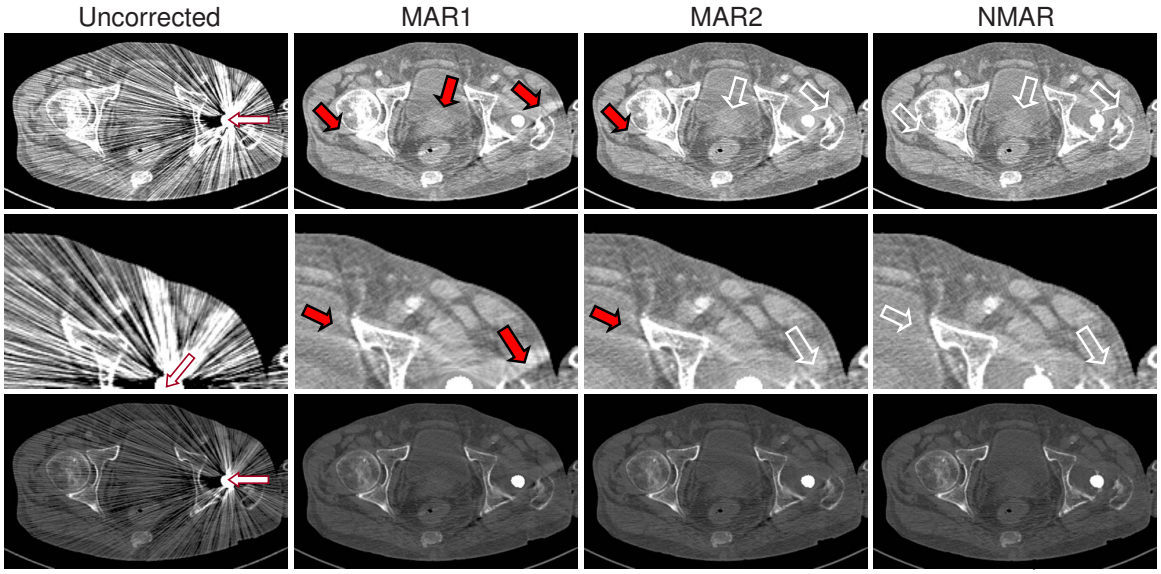

FIG. 7. Patient 2 with unilateral total hip endoprosthesis. Arrows in analogy to Fig. 5. All three MAR methods lead to better image quality. The single prosthesis with its round cross section is an ideal case for interpolation-based MAR. Compared to MAR1, both MAR2 and NMAR lead to a more homogeneous result and less artifacts tangent to the prosthesis. After correction with MAR2, dark artifacts close to bone structures are visible, which are avoided by NMAR. Top and middle row: (C=0 HU/W=750 HU). Bottom row: (C=500 HU/W=1500 HU).

IV.B.3. Patient 3

Three slices of patient 3, the patient with dental fillings, are presented in Figs. 10–12. Metal artifact reduction in the presence of dental fillings or crowns is especially challenging. There are often multiple metal objects of high density and irregular shape. Also, dental enamel is the densest material that is found naturally in the human body. The absolute error that can be made by interpolation is therefore higher than in other cases.

Figure 10 shows a slice through the lower jaw with a filling in a back tooth. Artifacts obscure the region of the tongue in large parts. The correction with MAR1 and MAR2 removes the strong streak artifacts as well as the excessive beam hardening artifacts. With NMAR, the image is restored even in regions close to the filling and the newly introduced artifacts are least prominent.

The slice presented in Fig. 11 can be almost regarded as a worst case scenario: Multiple dental fillings on both sides of

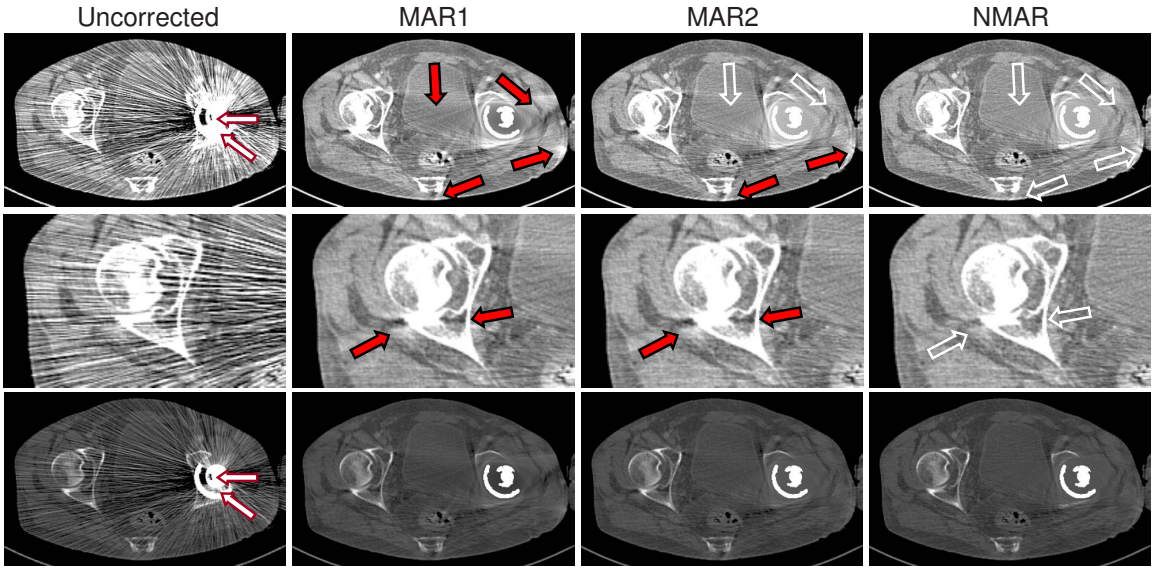

FIG. 8. Patient 2 with unilateral total hip endoprosthesis—shown is a slice with a greater metal cross section than in Fig. 7. Arrows in analogy to Fig. 5. Correction with MAR2 and NMAR leads to a more homogeneous result and less artifacts tangent to the prosthesis. As in Fig. 7, after correction with MAR2, dark artifacts close to bone structures are visible, which are avoided with NMAR. Top and middle row: (C=0 HU/W=750 HU). Bottom row: (C=500 HU/W=1500 HU).

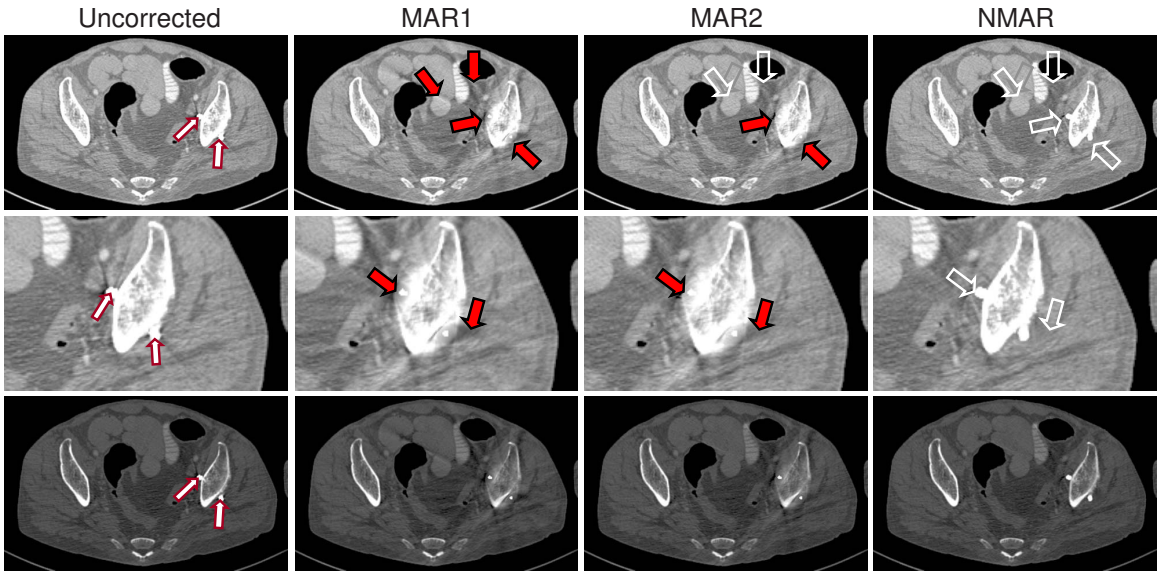

FIG. 9. Patient 2 with unilateral total hip endoprosthesis. Arrows in analogy to Fig. 5. The presented slice intersects the end of the fixation of the prosthesis. The artifacts in the uncorrected image are very mild. In the correction results for MAR1 and MAR2, the fine bone structures close to the fixation are blurred. In the NMAR corrected image, no blurring and no streak artifacts are visible. Top and middle row: (C=0 HU/W=750 HU). Bottom row: (C=500 HU/W=1500 HU).

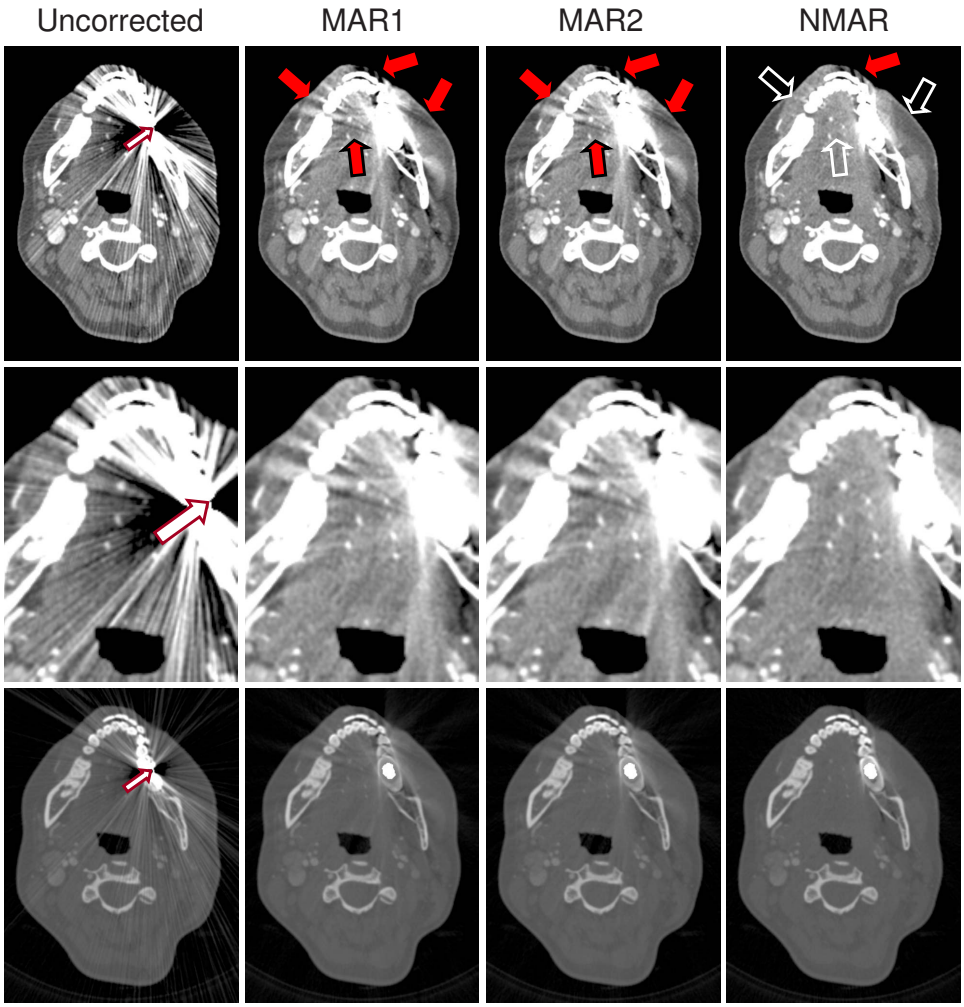

FIG. 10. Patient 3, slice through a dental filling in a molar in the lower jaw. Arrows in analogy to Fig. 5. In the uncorrected image, artifacts obscure large parts of the region of the tongue. The correction with MAR1 and MAR2 removes the strong streak artifacts as well as the excessive beam hardening artifacts, but some new streak artifacts and blurring are introduced. With NMAR, the image is restored even in regions close to the filling. Top and middle row: (C=100 HU/W=750 HU). Bottom row: (C=1000 HU/W=4000 HU).

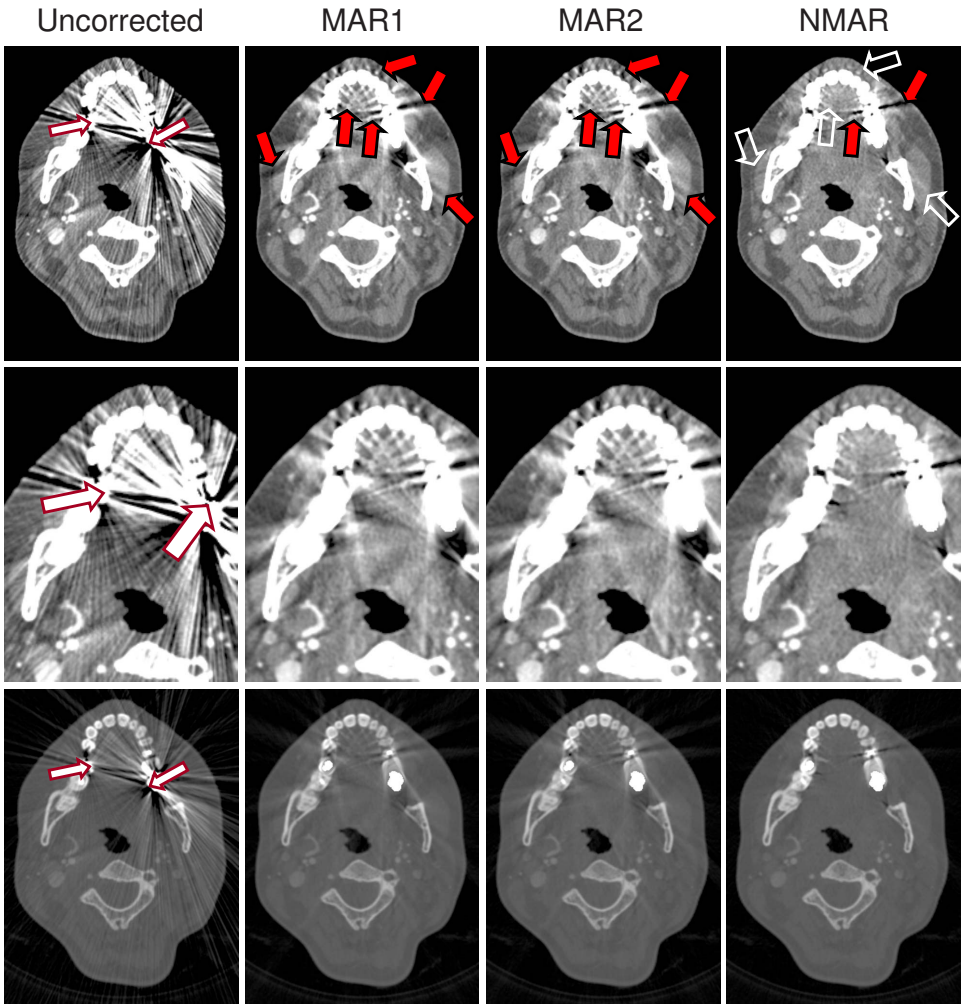

FIG. 11. Patient 3, with multiple dental fillings on both sides of the jaw. Arrows in analogy to Fig. 5. In the uncorrected image in the top row, anatomical features are hardly visible in the anterior part. Some artifacts can be removed with MAR1 and MAR2, but at the cost of new artifacts. Even with NMAR some artifacts remain in this worst case scenario. The remaining artifacts are much less strong compared to the artifacts introduced with MAR1 and MAR2, which impair large parts of the slice. The middle row shows a part of a reconstruction with a field of view of 100 cm. Top row and middle row: (C=100 HU/W=750 HU). Bottom row: (C=1000 HU/W=4000 HU).

the jaw. In the narrow window, anatomical features are hardly visible in the anterior part. Again, metal artifacts can be removed with MAR1 and MAR2 to some extent, but at the cost of new and severe interpolation artifacts. Unfortunately, even with NMAR, some artifacts remain. However, the result is better than with MAR1 and MAR2, which impair the image quality in large parts of the slice.

In the third slice, which is shown in Fig. 12, the lower end of a dental filling is intersected, which has only a small cross section. Fine streak artifacts are visible mostly in the posterior part. They can be removed with MAR1, MAR2, and NMAR, with MAR1 and MAR2 introducing new artifacts, mainly in the region of the teeth, whereas the result obtained with NMAR is free of artifacts.

IV.B.4. Patient 4

Results for patient 4 are shown in Fig. 13. The patient's spine is fixed with a Harrington rod. The metal rod has a relatively small cross section and causes fine streak artifacts and moderate beam hardening artifacts. MAR1 and MAR2 even impair the image quality. The right hand side transverse process of the vertebra is blurred and dark artifacts between bones appear after the correction with MAR1 or MAR2. NMAR corrects the metal artifacts while perfectly preserving the bone structures.

From this example, as well as from the results presented in Fig. 9 and 12, an important advantage of NMAR is found: Images from slices with only small metal implants, which only suffer from less severe artifacts, are not made worse than the uncorrected images. NMAR preserves all structures, as it uses the prior image, which is very accurate in these cases.

V. DISCUSSION

NMAR has shown to deliver promising results for different types of metal implants. However, the evaluation of the results for patient data in this work is of course subjective. By visual inspection, NMAR outperforms both other meth-

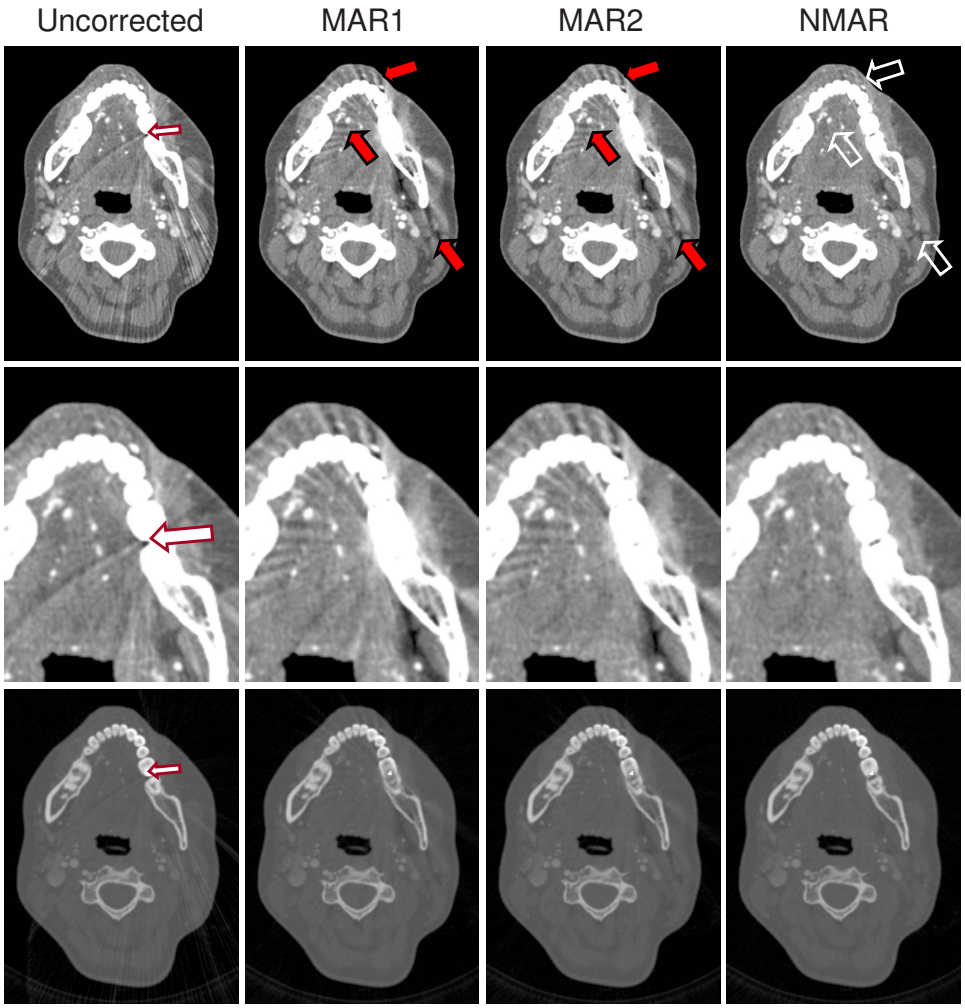

FIG. 12. Patient 3, slice through the lower end of a dental filling, which has only a small cross section. Arrows in analogy to Fig. 5. Fine streak artifacts are visible mostly in the posterior part. MAR1 and MAR2 introduce artifacts in the same order of magnitude as those which are removed. NMAR removes the artifacts and preserve all structures. Top and middle row: (C=100 HU/W=750 HU). Bottom row: (C=1000 HU/W=4000 HU).

ods. A quantitative assessment is problematic, as no ground truth is available for the patient data and results with phantoms are not fully transferable. To fully prove the effectiveness of this algorithm, a clinical study involving more cases and the systematic evaluation by trained radiologists is planned.

Finding a good prior image is an essential point of this algorithm. Faulty segmentation results can lead to residual artifacts, as seen in Fig. 11. A more advanced segmentation algorithm would surely enhance the results compared to simple thresholding, but this is out of the scope of this work. Patient 3 demonstrates the limitations of the proposed algorithm. If the prior image contains segmentation errors even after precorrection, residual artifacts are unavoidable. This is likely if there are too many or too big metal implants, and especially if those implants are close to bone. In this case, as seen in Fig. 11, the remaining artifacts are found in the NMAR result. Parts of the dark beam hardening artifacts were mistakenly segmented as air and some bright parts as bone. These wrong values were segmented from the MAR1 corrected image and the correction result therefore cannot be worse than this image. On the other hand, only artifacts in the MAR1 image that are severe enough to fall in a wrong tissue class will have a negative effect. Still, some streaks and blurring can be removed and the result is clearly better than the MAR1 result.

VI. CONCLUSION

Applying NMAR to simulation as well as clinical data yields excellent results. Even for high metal artifact content and close to metal implants, NMAR reduces artifacts in large part. In regions further away from metal implants, almost no artifacts remain after a correction with NMAR. While MAR2 performs better than MAR1 in some cases, NMAR performs better than MAR1 and MAR2 in all the cases that were considered in this work. For images with very small metal implants and few artifacts MAR1 and MAR2 can even reduce image quality, while NMAR delivers almost artifact-free results in these situations.

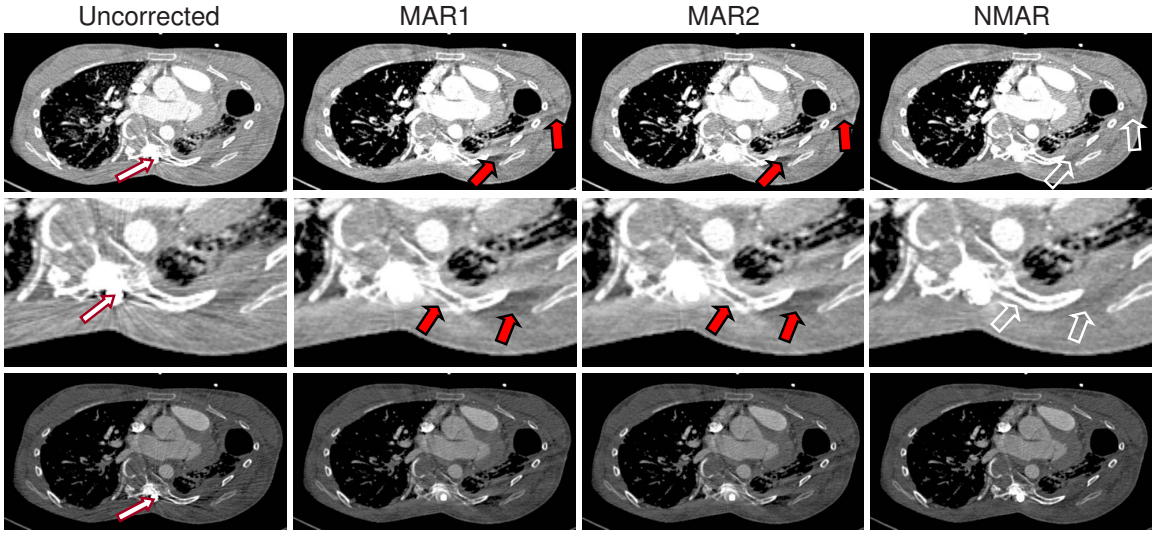

FIG. 13. Shown is patient 4 with a Harrington rod for spinal fixation. Arrows in analogy to Fig. 5. In the image, the rod is located below the vertebra. Fine streak artifacts and moderate beam hardening artifacts emerge from there. This patient with few metal and medium metal artifacts is an example where MAR1 and MAR2 even impair the image quality. The transverse process on the right hand side of the vertebra is blurred and dark artifacts between bones appear after correction with MAR1 or MAR2. NMAR corrects the metal artifacts while preserving the bone structures. Top and middle row: (C=0 HU/W=1000 HU). Bottom row: (C=500 HU/W=1500 HU).

VII. SUMMARY

Sinogram interpolation-based methods are the most common type of MAR methods, but they often introduce new artifacts because the full information from the metal shadow cannot be recovered. These artifacts are especially severe when high-contrast structures, for example, teeth, are present. To overcome this drawback, a generalized sinogram normalization technique is introduced and evaluated in this work. NMAR is designed to efficiently reduce metal artifacts and to prevent the introduction of new artifacts. The normalization is based on the 3D forward projection of a prior image, which is obtained by a multithreshold segmentation. The prior image models air, soft tissue, and bone regions. The normalized projections are subject to an interpolation-based MAR operation. In this work, NMAR is used with linear interpolation. Any interpolation scheme that is suitable for MAR could be chosen, but we did not find additional advantages of using more complex interpolation schemes for NMAR. The corrected sinogram is obtained by denormalization of the interpolated, normalized sinogram.

Results from four patients, with hip endoprostheses, dental fillings, and spine fixation are presented in this work. Three were scanned with a Somatom Definition Flash scanner at pitch values ranging from 0.9 to 3.2, one was scanned on a Somatom Sensation 16 scanner at pitch 1. NMAR reliably reduces metal artifacts in images reconstructed from simulated as well as from clinical data. Image quality, in general, is increased compared to MAR using linear interpolation and MAR with a simple length normalization. Details, especially close to metal objects and bones, are much better preserved. Compared to iterative methods, the presented method is computationally inexpensive and can be used as an additional step in conventional sinogram interpolation-based MAR methods. Even for patients with dental fillings, satisfactory results are obtained with the presented method, which is important as those patients with dental fillings make up the major part of patients with metal inside their body, and the artifacts are especially severe here.

Pure interpolation methods, as MAR1, disregard the information from the metal trace completely and lead to blurring close to metal implants. NMAR also completely replaces the metal trace, but by using the projections of the prior image, which contain information from the whole image, some of the information from the metal trace is used indirectly. MAR1 and MAR2 introduce some new artifacts in all the cases considered in this work. NMAR reduces artifacts even close to metal implants. In the case of mild to moderate artifacts, NMAR does not suffer from the loss of information close to implants. In these cases, almost no artifacts remain after a correction with NMAR in regions further away from metal implants. A clinical study involving more cases is planned to fully prove the effectiveness of the algorithm.

[a]Author to whom correspondence should be addressed. Electronic mail: esther.meyer@imp.uni-erlangen.de; Telephone: 49 (9131) 85 25535; Fax: 49 (9131) 85 22824.

[1]W. Kalender, *Computed Tomography: Fundamentals, System Technology, Image Quality, Applications* (Publicis, Erlangen, 2005).
[2]G. H. Glover and N. J. Pelc, "An algorithm for the reduction of metal clip artifacts in CT reconstructions," Med. Phys. **8**(6), 799–807 (1981).
[3]W. A. Kalender, R. Hebel, and J. Ebersberger, "Reduction of CT artifacts caused by metallic implants," Radiology **164**(2), 576–577 (1987).
[4]A. H. Mahnken, R. Raupach, J. E. Wildberger, B. Jung, N. Heussen, T. G. Flohr, R. W. Günther, and S. Schaller, "A new algorithm for metal artifact reduction in computed tomography: In vitro and in vivo evaluation after total hip replacement," Invest. Radiol. **38**(12), 769–775 (2003).
[5]J. Wei, L. Chen, G. A. Sandison, Y. Liang, and L. X. Xu, "X-ray CT high-density artifact suppression in the presence of bones," Phys. Med. Biol. **49**(24), 5407–5418 (2004).
[6]K. Y. Jeong and J. B. Ra, "Reduction of artifacts due to multiple metallic objects in computed tomography," Medical Imaging 2009: Physics of

Medical Imaging, Vol. 7258, p. 72583E, 2009 (unpublished).
[7]M. Bal and L. Spies, "Metal artifact reduction in CT using tissue-class modeling and adaptive prefiltering," Med. Phys. **33**(8), 2852–2859 (2006).
[8]D. Prell, Y. Kyriakou, M. Beister, and W. Kalender, "A novel forward projection-based metal artifact reduction method for flat-detector computed tomography," Phys. Med. Biol. **54**(21), 6575–6591 (2009).
[9]M. Kachelrieß, O. Watzke, and W. A. Kalender, "Generalized multi-dimensional adaptive filtering (MAF) for conventional and spiral single-slice, multi-slice and cone-beam CT," Med. Phys. **28**(4), 475–490 (2001).
[10]M. Bal, H. Celik, K. Subramanyan, K. Eck, and L. Spies, "A radial adaptive filter for metal artifact reduction," Proc. SPIE **5747**, 2075–2082 (2005).
[11]G. Wang, D. L. Snyder, J. A. O'Sullivan, and M. W. Vannier, "Iterative deblurring for CT metal artifact reduction," IEEE Trans. Med. Imaging **15**(5), 657–664 (1996).
[12]B. De Man, J. Nuyts, P. Dupont, G. Marchal, and P. Suetens, "An iterative maximum-likelihood polychromatic algorithm for CT," IEEE Trans. Med. Imaging **20**(10), 999–1008 (2001).
[13]M. Oehler and T. M. Buzug, "Modified MLEM algorithm for artifact suppression in CT," IEEE Medical Imaging Conference Record, Vol. M16-1, pp. 3511–3518, 2006 (unpublished).
[14]C. Lemmens, D. Faul, and J. Nuyts, "Suppression of metal artifacts in CT using a reconstruction procedure that combines MAP and projection completion," IEEE Trans. Med. Imaging **28**(2), 250–260 (2009).
[15]O. Watzke and W. A. Kalender, "A pragmatic approach to metal artifact reduction in CT: Merging of metal artifact reduced images," Eur. J. Radiol. **14** (5), 849–856 (2004).
[16]X. Duan, L. Zhang, J. Xiao, J. Cheng, Z. Chen, and Y. Xing, "Metal artifact reduction in CT images by sinogram TV inpainting," Nuclear Science Symposium Conference Record, 2008 (NSS '08), pp. 4175–4177 (unpublished).
[17]J. Müller and T. M. Buzug, "Spurious structures created by interpolation-based CT metal artifact reduction," Proc. SPIE **7258**(1), 1Y1–1Y8 (2009).
[18]M. Oehler and T. M. Buzug, "Statistical image reconstruction for inconsistent CT projection data," Methods Inf. Med. **3**, 261–269 (2007).
[19]B. Kratz and T. M. Buzug, "Metal artifact reduction in computed tomography using nonequispaced Fourier transform," IEEE Medical Imaging Conference Record, pp. 2720–2723, 2009 (unpublished).
[20]L. Yu, H. Li, J. Mueller, J. Kofler, X. Liu, A. Primak, J. Fletcher, L. Guimaraes, T. Macedo, and C. McCollough, "Metal artifact reduction from reformatted projections for hip prostheses in multislice helical computed tomography: Techniques and initial clinical results," Invest. Radiol. **44**(11), 691–696 (2009).
[21]W. J. H. Veldkamp, R. M. S. Joemai, A. J. van der Molen, and J. Geleijns, "Development and validation of segmentation and interpolation techniques in sinograms for metal artifact suppression in CT," Med. Phys. **37**(2), 620–628 (2010).
[22]E. Meyer, F. Bergner, R. Raupach, T. Flohr, and M. Kachelrieß, "Normalized metal artifact reduction (NMAR) in computed tomography," Nuclear Science Symposium Conference Record (NSS/MIC) 2009 IEEE, pp. 3251–3255, 2009.
[23]P. M. Joseph, "An improved algorithm for reprojecting rays through pixel images," IEEE Trans. Med. Imaging **1**(3), 192–196 (1982).
[24]D. Prell, Y. Kyrikou, T. Struffert, A. Dörfler, and W. A. Kalender, "Metal artifact reduction for clipping and coiling in interventional C-arm CT," AJNR Am. J. Neuroradiol. **31** (4), 634–639 (2010).